J Mater Sci (2007) 42:9855–9858
DOI 10.1007/s10853-007-1799-z

Synthesis of antimony oxide nano-particles by vapor transport and condensation

C. H. Xu · S. Q. Shi · C. Surya · C. H. Woo

Received: 7 February 2007 / Accepted: 23 April 2007 / Published online: 18 August 2007

Abstract This paper reports the synthesis of Sb_2O_3 nano-particles by vapor transport and condensation of metallic antimony in oxidizing environment. Granular antimony inside an alumina crucible is placed in the middle of a tube furnace at 550 °C with air flow rate of 400 mL/min. Al foil, glass and Si-wafer, which are used as substrates, are placed downstream of the gas flow at a temperature of about 250 °C for the deposition of antimony oxide. The deposited antimony oxides on the substrates and the oxidized granular antimony in the alumina crucible are examined with field emission scanning electron microscopy, X-ray diffractometer and transmission electron microscopy (TEM). The deposited antimony oxide consists of Sb_2O_3 nano-particles, while the oxidized granular antimony in the crucible consists of SbO_2. The mechanism of the formation of Sb_2O_3 nano-particles is analyzed based on oxidation reaction thermodynamics and kinetics.

Introduction

Nano-materials have attracted much attention over the past decade as a material form for scientific research and technological applications due to their novel or even outstanding properties compared to bulk materials. Semiconducting nano-particle materials have been an area of intense investigation on the synthesis, structures and properties. One particularly interesting aspect is the investigation of semiconducting metal oxide nano-particles [1, 2]. Antimony oxide is useful as a catalyst, retardant and optical materials [3]. Recently, antimony oxide is found to have high proton conductivity, making it potentially useful as a humidity-sensing materials [4, 5]. In fact, Sb_2O_3 [6] and Sb_2O_3 plus ZnO [7] have been used to make films for gas sensing purposes.

It was reported recently that the synthesis of antimony oxide nano-particles can be achieved via the chemical method [8], hydrolysis-precipitate method [9] and γ-ray radiation–oxidation route [10], in which $SbCl_3$ is used as the starting material. Another reported method for the synthesis of antimony oxide nano-particles is the formation of plasma on liquid metal antimony which is heated under a flowing Ar + O_2 atmosphere by an inductive resource and laser beam [11, 12]. However, only a mixture of Sb and antimony oxide nano-particles is usually obtained this way.

In this paper we report the synthesis of antimony oxide nano-particles by heating metal antimony in the solid state in a tube furnace with an oxidizing environment. Antimony oxide is deposited on a substrate at the downstream of gas flow. Comparing to the technique outlined in references [11, 12], the present process is capable of synthesis of pure Sb_2O_3 nano-particles in a more cost effective manner. The mechanism for the formation of pure Sb_2O_3 phase is explained by the oxidation reaction thermodynamics and kinetics.

Experimental procedure

The experimental setup for the synthesis of antimony oxide nano-particles by vapor transport and condensation

C. H. Xu (✉) · S. Q. Shi
Department of Mechanical Engineering, Hong Kong Polytechnic University, Hung Hom, Kowloon, Hong Kong, China
e-mail: mmcjxu@yahoo.com.au

C. Surya · C. H. Woo
Department of Electronic and Information Engineering, The Hong Kong Polytechnic University, Hung Hom, Kowloon, Hong Kong, China

is illustrated in Fig. 1. Commercial granular antimony with average diameter of 1.5 mm (purity: 99.99% Sb) is placed in an alumina crucible in the middle of a tube furnace in compressed air at 1 atmosphere pressure, with a constant flow rate of 400 mL/min. Two different deposition times of 4 h and 20 h are used in our investigation. The temperature in the middle of the furnace is set at 550 °C (melting point of Sb is 630.5 °C). The substrates, including Al foil, glass and Si-wafer, are placed in the downstream of the gas flow, where the temperature is kept at 250 °C for the deposition of antimony oxide.

The crystal structures of the original granular antimony, the oxidized granular antimony in the alumina crucible and the deposited antimony oxides on the substrates are examined with a Philips PW3710 X-ray diffractometer, using a 40 kV, 30 mA, CuKα X-ray. A field-emission scanning electron microscope (JEOL JSM-6335F) is also used to characterize the morphologies of the oxide. After the deposition time of 4 h, a piece of the Al foil with the deposited oxide is placed in a test tube with ethanol. The ethanol solution is placed in an ultrasonic machine (COLE-Parmer 8890) for 10 min to separate the oxides from the Al foil. Then the resulting solution is dropped onto a carbon coated transmission electron microscopy (TEM) copper grid. TEM imaging, electron diffraction and local composition analysis are performed on the samples on the TEM grid using a JEOL 2010F TEM with an energy dispersive spectroscopy (EDS) system, operated at 200 kV.

Experimental results

Both the deposited oxide on the substrates and the oxidized granular antimony in the alumina crucible are white in color. The nano-particles deposited on the different substrates have similar features. After a deposited time of 4 h, the size of nano-particles on the Al foils ranges between 10 nm and 100 nm (Fig. 2a). The particles have triangular, hexagonal and rectangular shapes with well-defined crystal structures. The size of nano-particles increases with the deposition time. As shown in Fig. 2b, the size of the pile of antimony oxides is about 150–250 nm after the deposition of 20 h.

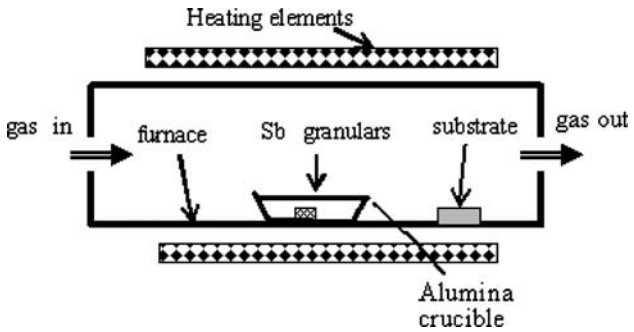

Fig. 1 Experimental setup shows the positions of granular antimony and the substrates

X-ray diffraction results are show in Fig. 3. An X-ray spectrum of the original granular antimony shows metallic antimony with a rhombohedral structure in Fig. 3a. The oxidized granular antimony in the alumina crucible after the deposition of 4 h exhibits an orthorhombic phase of SbO_2 (Fig. 3b). Figure 3c shows the XRD spectrum of the oxide deposited on the Al foil for 4 h. The metallic Al peaks can be clearly identified from the spectrum. Only one peak on the spectrum belongs to the oxide present in a small amount and the phase of the oxide cannot be identified. Oxide particles deposited on Al foil after the reaction of 20 h are also examined, and the corresponding XRD spectrum is shown in Fig. 3d. It can be seen that the oxide has the face-centered cubic structure of Sb_2O_3. Comparing Fig. 3a and d, it can be concluded that metallic antimony is not present in the oxide particles.

The TEM images in Fig. 4 show that the grain size ranges from 10 nm to 100 nm. Figure 4a shows a pile of antimony oxides (right) and the corresponding electron diffraction pattern (left). All rings can be indexed to the diffraction peaks of face-centered cubic Sb_2O_3. A large grain, which is almost-triangular in shape, is shown in Fig. 4b. The corresponding electron diffraction pattern, as illustrated on the right-hand side, comes from {440} of Sb_2O_3, suggesting that the triangular surface is the (111) surface of Sb_2O_3. A high resolution image taken on the triangular Sb_2O_3 corresponds to the (440) plane of Sb_2O_3 shows a lattice space of 1.95 Å. An EDS analysis on the nano-particles shows the presence of both Sb and O elements.

Discussions

From Fig. 3, the phase of the deposited oxide on the substrates is different from the oxidized granular antimony in the alumina crucible, which is explained as following. The oxides deposited on Al-foil substrates placed downstream of an alumina crucible in which metal antimony is oxidized in flowing air at the temperature of 550 °C are found to be Sb_2O_3. The metallic antimony in the alumina crucible is found to be oxidized as SbO_2 after the reaction. According to the Sb–O phase diagram [13], well identified antimony oxides are mainly Sb_2O_3, SbO_2, Sb_2O_5. According to the theory of oxidation [14, 15, 16], the condition of the formation of antimony oxides in oxidizing environment is governed by the following equations:

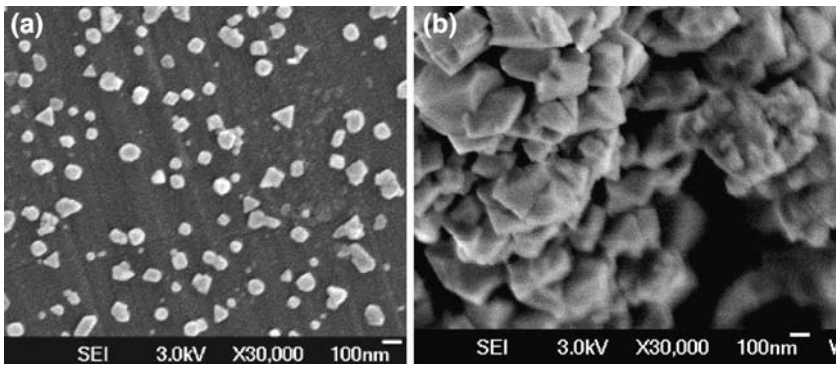

Fig. 2 Morphologies of the deposited antimony oxides on Al-foil substrate, showing size of nano-particles (**a**) about 10–100 nm after the reaction of 4 h, and (**b**) 150–250 nm after the reaction of 20 h

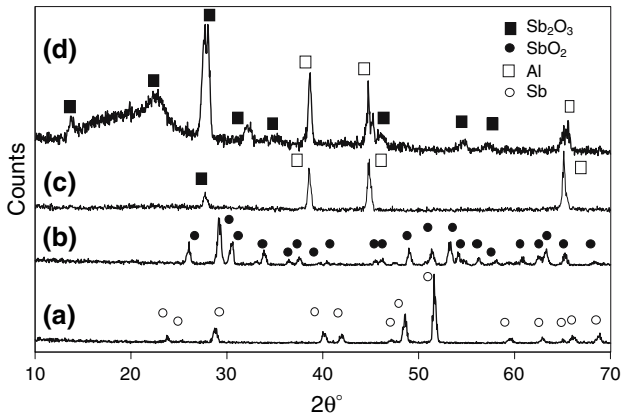

Fig. 3 X-ray spectra (**a**) granular antimony before the reaction, (**b**) the oxidized granular antimony in the alumina crucible after the reaction of 4 h, showing SbO_2 oxide, (**c**) the deposited oxide on Al-foil after the reaction of 4 h, and (**d**) the deposited oxide on Al-foil after the reaction of 20 h, showing Sb_2O_3 oxide

$$\frac{4}{3}\mathrm{Sb} + \mathrm{O_2} = \frac{2}{3}\mathrm{Sb_2O_3} \quad \Delta G_1^0 = -466406.9 + 183.991\mathrm{T\ (J)}$$

$$P_{\mathrm{O_2}}^{\mathrm{eq}}(\mathrm{Sb_2O_3}) = \frac{(a_{\mathrm{oxide}})^{\frac{2}{3}}}{(a_{\mathrm{Sb}})^{\frac{4}{3}}}\exp\frac{\Delta G_1^0}{RT} \tag{1}$$

$$\mathrm{Sb} + \mathrm{O_2} = \mathrm{SbO_2} \quad \Delta G_2^0 = -447990 + 187.188\mathrm{T\ (J)}$$

$$P_{\mathrm{O_2}}^{\mathrm{eq}}(\mathrm{SbO}) = \frac{(a_{\mathrm{oxide}})}{(a_{\mathrm{Sb}})}\exp\frac{\Delta G_2^0}{RT} \tag{2}$$

$$\frac{4}{5}\mathrm{Sb} + \mathrm{O_2} = \frac{2}{5}\mathrm{Sb_2O_5} \quad \Delta G_3^0 = -403272 + 191.614\mathrm{T\ (J)}$$

$$P_{\mathrm{O_2}}^{\mathrm{eq}}(\mathrm{Sb_2O_5}) = \frac{(a_{\mathrm{oxide}})^{\frac{2}{5}}}{(a_{\mathrm{Sb}})^{\frac{4}{5}}}\exp\frac{\Delta G_3^0}{RT} \tag{3}$$

where ΔG^0 is the Gibbs energy change in oxidation reactions when all species are present in their standard states. a_{oxide} and a_{Sb} are the thermodynamic activities of the oxides and metal, respectively (the thermodynamic activity of pure metal or pure oxide is equal to 1). $P_{\mathrm{O_2}}^{\mathrm{eq}}$ is the equilibrium pressure of oxygen in the related oxidation reaction. R is the gas constant and T is absolute temperature. Sb_2O_5 does not form above 525 °C, so we only consider the formation of Sb_2O_3 and SbO_2 at 550 °C. Based on the Gibbs energies [17], in Eqs. 1 and 2, the equilibrium pressures of oxygen ($P_{\mathrm{O_2}}^{\mathrm{eq}}$) for Sb_2O_3 and SbO_2 at 550 °C can be calculated as 9.94×10^{-21} and 2.16×10^{-19} atm., respectively. According to the theory of oxidation, when more than one type of oxides co-exist with the metal in the system, a multilayer scale forms on the

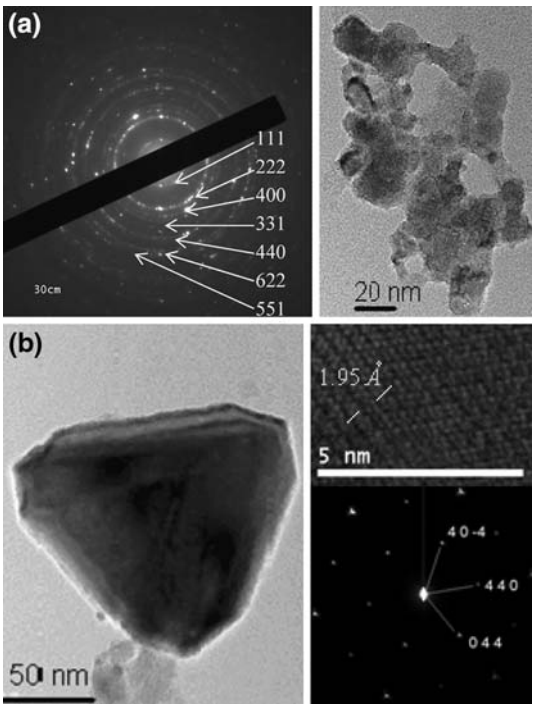

Fig. 4 TEM images for Sb_2O_3 oxide particles (**a**) the morphology of a pile of antimony oxides (right) and the corresponding electron diffraction (left), indexing all rings to the diffraction peaks of face-centered cubic Sb_2O_3, and (**b**) the morphology of a large triangle grain (left), the corresponding selected area electron diffraction pattern (right bottom) and the related high resolution image taken on the triangle Sb_2O_3 (right top)

metal, consisting of oxides of varying oxygen content, from metal-rich oxides with a low oxygen equilibrium pressure to oxygen-rich oxides with a high oxygen equilibrium pressure [16]. The composition of the oxide is thus sequentially metallic antimony, Sb_2O_3 and SbO_2, as illustrated in Fig. 5a. The outermost layer that is composed of the SbO_2 phase is most easily detected by XRD (see Fig. 3b), because the signal of the diffraction mainly comes from the top 10 μm of the tested material [18].

The size of the nano-oxide particles deposited on the substrates is in the range of 10–100 nm after reaction of 4 h. The TEM in Fig. 4 and XRD results in Fig. 3 indicate that the deposited oxide on the substrate is cubic Sb_2O_3. Vapor evaporation and condensation can be used to account for the formation of Sb_2O_3 nano-particles. Metallic antimony or SbO_2 evaporates from the samples in the alumina crucible. The Sb or SbO_2 vapor flows with flowing air. At same time, the Sb or SbO_2 are further oxidized in air to form the most stable oxide. Sb_2O_3, SbO_2, Sb_2O_5 oxides may form at temperatures below 525 °C according to Eqs. 1–3. The condensation temperature on the Al foil is about 250 °C. According to Eqs. 1–3 [17], the Gibbs energies changes for Sb_2O_3, SbO_2, Sb_2O_5 oxides at 250 °C can be calculated as −372030, −350090 and −303058 J. As the species with the lowest Gibbs energy (see Fig. 5b), Sb_2O_3 nano-particles form on the Al foil (Fig. 3c, d).

Formation of pure Sb_2O_3 nano-particles can be controlled by chemical reaction kinetics. If the rate of Sb vapor deposition is equal or less than that of oxidation, pure oxide can be obtained. Otherwise, a mixture of metal and oxide can be formed. It has been reported that by inductive-laser melting metallic antimony to form plasma in an oxidizing environment Sb_2O_3 nano-particles can be synthesized. This technique includes three steps: melting Sb by the inductive-laser source; oxidizing Sb vapor; and condensing antimony oxide on a water-cooled wall [11]. A mixture of Sb and Sb_2O_3 nano-particles is usually obtained by this method, and the nano-particles show the morphology of spheres. In terms of kinetic considerations, the formation of the nano-particles is perhaps a non-equilibrium process controlled by the high evaporation rate of the melting of the metal and the fast condensation of the oxide on a water-cooled wall.

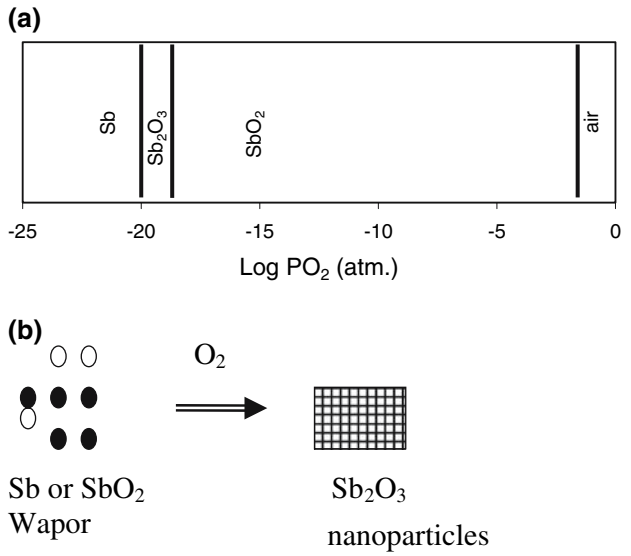

Fig. 5 Illustration of the formation of (**a**) a multilayer scale on granular antimony, and (**b**) Sb_2O_3 nano-particles on Al-foil

Conclusions

In summary, pure Sb_2O_3 nano-particles can be synthesized by heating metallic antimony at 550 °C in air at 1 atmosphere pressure with a flow rate of 400 mL/min. The vapor oxides are deposited on a substrate at the downstream of gas flow. The nano-particles are characterized by well-defined crystalline cubic Sb_2O_3. The size of the Sb_2O_3 nano-particles can be controlled in the range of 10–100 nm for the deposition time of 4 h. Formation of pure Sb_2O_3 phase is controlled by reaction thermodynamics and kinetics.

Acknowledgements This work was funded by Research Grant Council of Hong Kong (B-Q747, A-PG59), Research grant from PolyU G-U344, PolyU 5312/03E and PolyU 5236/03E.

References

1. Han WQ, Fan SS, Li QQ, Hu YD (1997) Science 277:1287
2. Morales AM, Liber CM (1988) Science 279:208
3. Samsonov GV (1973) The oxide handbook. IFI/Plenum
4. Ozawa K, Sakka Y, Amamo A (1998) J Mater Res 13:830
5. Dzimitrowice DJ, Goodenough JB, Wiseman PJ (1982) Mater Res Bull 17:971
6. Binions R, Carmalt CJ, Parkin IP (2006) Polyhedron 25:30323
7. Zhu BL, Xie CS, Wang AH, Zheng DW, Hu ML, Wang WY (2004) Mater Res Bull 39:409
8. Zhang ZL, Guo L, Wang WD (2001) J Mater Res 16:803
9. Hu YH, Zhang HH, Yang HM (2007) J Alloys Compd 428:327
10. Liu YP, Zhang YH, Zhang MW, Zhang WH, Qian YT, Yang L, Wang CS, Chen ZW (1997) Mater Sci Eng B 49:42
11. Zeng DW, Zhu BL, Xie CS, Song WL, Wang AH (2004) Mater Sci Eng A 366:332
12. Xie CS, Hu JH, Wu R, Xia H (1999) Nanostruct Mater 11:1061
13. Massalski TB, Okamoto H, Subramanian PR, Kacprzak L (eds) (1990) Binary alloy phase diagrams. ASM International, Materials Park
14. Xu CH, Gao W, He YD (2000) Scripta Mater 42:975
15. Xu CH, Woo CH, Shi SQ (2004) Chem Phys Lett 399:62–66
16. Khanna AS (2002) Introduction to high temperature oxidation and corrosion. ASM International, USA
17. Samsonov GV (1982) The oxide handbook. IFI/Plenum, New York
18. Brundle CR, Evans CA, Wilson JS (1992) Encyclopedia of materials characterization: surface, interface, thin film. Butterworth-Heinemann, USA